

ASTROMETRIC POSITIONS AND PROPER MOTIONS OF 19 RADIO STARS

D. A. BOBOLTZ¹, A. L. FEY¹, K. J. JOHNSTON¹, M. J. CLAUSSEN², C. DE VEGT^{3,4}, N. ZACHARIAS¹, AND
R. A. GAUME¹

Accepted by the Astronomical Journal 2003 March 18

ABSTRACT

We have used the Very Large Array, linked with the Pie Town Very Long Baseline Array antenna, to determine astrometric positions of 19 radio stars in the International Celestial Reference Frame (ICRF). The positions of these stars were directly linked to the positions of distant quasars through phase referencing observations. The positions of the ICRF quasars are known to 0.25 mas, thus providing an absolute reference at the angular resolution of our radio observations. Average values for the errors in our derived positions for all sources were 13 mas and 16 mas in $\alpha \cos \delta$ and δ respectively, with accuracies approaching 1–2 mas for some of the stars observed. Differences between the ICRF positions of the 38 quasars, and those measured from our observations showed no systematic offsets, with mean values of -0.3 mas in $\alpha \cos \delta$ and -1.0 mas in δ . Standard deviations of the quasar position differences of 17 mas and 11 mas in $\alpha \cos \delta$ and δ respectively, are consistent with the mean position errors determined for the stars. Our measured positions were combined with previous Very Large Array measurements taken from 1978–1995 to determine the proper motions of 15 of the stars in our list. With mean errors of ≈ 1.6 mas yr⁻¹, the accuracies of our proper motions approach those derived from Hipparcos, and for a few of the stars in our program, are better than the Hipparcos values. Comparing the positions of our radio stars with the Hipparcos catalog, we find that at the epoch of our observations, the two frames are aligned to within formal errors of approximately 3 mas. This result confirms that the Hipparcos frame is inertial at the expected level.

Subject headings: astrometry — binaries: close — radio continuum: stars — techniques: interferometric

1. INTRODUCTION

The current realization of the International Celestial Reference Frame (ICRF) is defined by the positions of 212 extragalactic objects derived from Very Long Baseline Interferometry (VLBI) observations (Ma et al. 1998). This VLBI realization of the ICRF is currently the International Astronomical Union (IAU) sanctioned fundamental astronomical reference frame. At optical wavelengths, the Hipparcos catalog (Perryman et al. 1997) now serves as the primary realization of the extragalactic frame. The link between the Hipparcos catalog and the ICRF was accomplished through a variety of ground-based and space-based efforts (Kovalevsky et al. 1997) with the highest weight given to VLBI observations of 12 radio stars by Lestrade et al. (1999). The standard error of the alignment was estimated to be 0.6 mas at epoch 1991.25, with an estimated error in the system rotation of 0.25 mas yr⁻¹ per axis. Thus at the epoch of our observations (2000.94) the alignment of the Hipparcos frame and the ICRF had a formal error of approximately 2.5 mas. Due to errors in the proper motions, the random position errors of individual Hipparcos stars increased from ~ 1 mas in 1991 to ~ 10 mas at the time of our observations. Upcoming astrometric satellite missions such as SIM and GAIA will likely define frames with internal accuracies that are better than the extragalactic VLBI frame by an order of magnitude, and these frames may define the next generation ICRF.

In this paper, we present our observations of 19 radio stars using the Very Large Array (VLA) in A configuration linked by fiber optic transmission line to the Very Long Baseline Array (VLBA) antenna located in Pie Town, New Mexico. Both

the VLA and VLBA are maintained and operated by the National Radio Astronomy Observatory (NRAO)⁵. The VLA plus Pie Town (VLA+PT) link (Claussen et al. 1999) is a valuable tool for radio star astrometry because it provides the high sensitivity of the VLA with nearly twice the resolution of the VLA A-configuration alone for high declination sources. In sections 2 and 3 we describe the observations, reduction of the data, and the methodology used in the determination of source positions and associated errors. The observations described here represent a continuation of a long-term program (since 1978) to obtain accurate astrometric radio positions, parallaxes, and proper motions for ~ 50 radio stars, which can be used to connect the current ICRF to future astrometric satellite reference frames. In section 5 we combine our VLA+PT positions with previous positions derived from VLA data collected from 1978 through 1995 (Johnston et al. 1985; Johnston, de Vegt & Gaume 2003). We derive updated estimates of the proper motions for 15 of the stars observed in both programs, and compare these proper motions with the corresponding Hipparcos values.

2. OBSERVATIONS AND REDUCTION

The VLA+PT X-band observations occurred over a 24-hour period beginning 2000 December 10 at 06:30 LST. The data were recorded in dual circular polarization using two adjacent 50-MHz intermediate frequencies (IF's) centered on rest frequencies of 8460.1 MHz and 8510.1 MHz respectively. The distribution on the sky of the 19 radio stars observed is shown in Figure 1. For each star, two nearby ICRF reference sources were observed for phase calibration (see Table 1). The input

¹ U.S. Naval Observatory, 3450 Massachusetts Ave., NW, Washington, DC 20392-5420

² National Radio Astronomy Observatory, P.O. Box O, Socorro, NM 87801

³ Hamburger Sternwarte, Universitat Hamburg, Gojenbergsweg 112, D-201029 Hamburg, Germany

⁴ Deceased, 2002 July 12.

⁵ The National Radio Astronomy Observatory is a facility of the National Science Foundation operated under cooperative agreement by Associated Universities, Inc.

positions for the stars were Hipparcos values updated to the epoch of our observations using the Hipparcos proper motions and parallaxes. Input positions for the ICRF reference sources were those given in IERS Annual Report (1999). Because radio stars are generally weak (on the order of a few mJy) and because the goal of our observations was astrometry, negating the use of phase self calibration, we used the fast-switching technique (Carilli & Holdaway 1997) to observe the star and its primary phase calibrator in an attempt to mitigate phase fluctuations due to the atmosphere/ionosphere. Each fast-switched scan was bracketed by two short scans of a second ICRF source which was used as a phase calibration back-up and as a check for the accuracy of the position estimation. Over the 24-hour experiment, three observations of each radio star were conducted at three different hour angles in order to maximize the uv coverage. For the discussion presented here, an observation is defined as consisting of a short 1.5 minute scan on the secondary phase calibrator, followed by 17.6 minutes of fast switching between the star and the primary phase calibrator with a 2.5 minute cycle time (100 seconds on the star and 50 seconds on the calibrator), followed by a final 1.5 minute scan on the secondary phase calibrator. In addition, two 5 minute scans were recorded on the sources 3C48 and 3C147 for use in the absolute flux density calibration.

Data were reduced using the standard routines within the Astronomical Image Processing System (AIPS). The absolute flux density scale was established using the values calculated by AIPS for 3C48 and 3C147 (3.22 Jy and 4.81 Jy respectively) with the proper uv restrictions applied. For each star, two calibrated uv data sets were generated. For the first, the phase calibration was accomplished through transfer of the phases of the primary (fast-switched) reference source. A second uv data set was generated for each star by applying the phases of the second ICRF calibrator (not fast-switched) bracketing the corresponding star. Each ICRF reference source was phase calibrated with the other reference source observed, i.e. the primary was calibrated using the secondary and the secondary calibrated using the primary. At no time was self-calibration performed on any of the data. From the uv data sets (two per star and one per calibrator), a set of five images were generated for each source: one CLEANed image including all observations, one dirty image with all observations, and three dirty images one per observation at the three different hour angles. Synthesized beam sizes ranged from approximately $0''.35 \times 0''.15$ for a source at a declination of -28° to $0''.17 \times 0''.14$ for a source at a declination of $+45^\circ$. The images produced have 512×512 pixels with a pixel size of $0''.015$. For the CLEANed images 100 iterations were used. A two-dimensional (2-D) Gaussian function was fit to the peak flux in each image using the AIPS task JMFIT. The results of these fits were used in the derivation of source positions described in the next section.

3. POSITION DETERMINATION

Final estimation of the star and calibrator positions was performed outside of AIPS using the results of the 2-D Gaussian fits to the various images. Peak and RMS flux densities for each source were derived from the fits to the CLEANed images. To avoid any possible position shifts due to CLEANing of the images, positions in right ascension and declination were determined from fits to the dirty images produced from the combined data for each source. A later comparison showed less than 1–2 mas differences between the positions derived from the dirty

and CLEANed images in all but one case. The star B Per, the lowest flux density source observed, had a difference in right ascension of 5 mas, which was still well within the position error reported for this source. Table 2 lists the positions and flux densities determined from the fits to the images of the 19 stars and their associated calibrator sources. Other than the tropospheric delay correction made by the VLA on-line system, which assumes a plane parallel slab model based on pressure, temperature and relative humidity measurements made at the VLA, no other correction was made for tropospheric/ionospheric effects. Figure 2 plots the position formal errors (as determined by JMFIT) in $\alpha \cos \delta$ and δ as a function of source elevation for all calibrator and target source observations. As seen in the figure, there is a small rise in position error for sources observed at elevations below about 25° . We made no attempt to model this phenomenon, but we did attempt to estimate contributions to the position errors due to tropospheric/ionospheric effects, as discussed below.

Documentation for the AIPS task JMFIT states that the errors in the position estimates should be regarded as tentative. Taking a conservative approach to error determination, we computed a root-sum-square combination of two separate error estimates. The first estimate, which is associated with the fitting of a 2-D Gaussian function to an image peak, is given by $\sigma \approx \theta_{beam} / 2SNR$, where SNR is the signal-to-noise ratio in the CLEANed image and θ_{beam} represents the geometric mean of the synthesized beam. The second estimate, which provides a measure of the uncertainty due to the changing troposphere/ionosphere, is a weighted root-mean-square (WRMS) position error computed in the following manner. For each individual observation, positions and associated errors in right ascension and declination were determined from a 2-D fit to the dirty images at three different hour angles. A WRMS position uncertainty was then computed for each source, with the individual position errors reported by JMFIT used as weights. The final errors reported in Table 2 are the combined root-sum-square of the two separate estimates. For most of the stars in our observations, the final reported errors were dominated by the WRMS uncertainties in the positions, with the errors due to Gaussian fitting being a small contributor.

For three of the stars in Table 2, HD50896-N, RS CVn, and HR5110, phase stability was found to be better using the secondary ICRF calibrator rather than the primary (fast-switched) calibrator as the phase reference source. Therefore, the positions and errors reported for these stars are from the data which were phase-calibrated using the secondary (not fast-switched) reference source. Mean values for the position errors for all 19 stars are 10 msec in right ascension, α , (13 mas in $\alpha \cos \delta$) and 16 mas in declination, δ . Upon close inspection of Table 2, it is obvious that the errors associated with the star HD50896-N and its two calibrator sources are substantially higher than errors for all of the other sources. This star was the second lowest declination star in our list, and its primary phase calibrator was the lowest declination source observed. In addition, one of the scans on this source was taken at a very low elevation (star at $\approx 16^\circ$ and primary phase calibrator at $\approx 11^\circ$). Disregarding HD50896-N and its associated calibrator sources, decreases the mean errors in the positions for all sources to 12 mas in both $\alpha \cos \delta$ and δ .

The lower limit on the accuracy of the positions for the best ICRF calibrators is 0.25 mas (Ma et al. 1998), well below the precision obtained from our VLA+PT measurements discussed

above. The ICRF coordinates thus provide representative reference positions with which to compare our VLA+PT positions. Figures 3 and 4 display the results of such a comparison. Differences between the ICRF positions and the VLA+PT positions for the calibrator sources are plotted as a function of source right ascension in Figure 3 and as a function of source declination in Figure 4. Error bars in the two figures are those derived for our VLA+PT measurements reported in Table 2. Neither figure shows a clear dependence of position offset on source right ascension or declination. The means of the differences in $\alpha \cos \delta$ and δ are -0.3 mas and -1.0 mas respectively, indicating that systematic effects are negligible. The standard deviations of the position differences are 17 mas and 11 mas in $\alpha \cos \delta$ and δ respectively. These values are roughly equivalent to the mean position errors for the stars derived above. If we again disregard the two calibrator sources associated with the star HD50896-N then the standard deviations of the differences fall to 10 mas in both $\alpha \cos \delta$ and δ .

4. RADIO/OPTICAL FRAME ALIGNMENT

In addition to the comparison of calibrator positions, we also compared the positions of the 19 stars as derived from our VLA+PT observations with the corresponding Hipparcos positions updated to the epoch of our observations, Julian Day 2451889. Figures 5 and 6 plot the position differences for the radio stars as a function of source right ascension (Figure 5) and as a function of source declination (Figure 6). Error bars are those derived from our VLA+PT observations. From Figures 5 and 6, it is apparent that roughly half of the positions derived from our VLA+PT data do not agree with the Hipparcos positions to within the uncertainties in our measurements. The most obvious disagreement is for the star UX Ari, for which the differences in $\alpha \cos \delta$ and δ are 84 mas and 42 mas respectively. The large offsets for UX Ari are real, and are discussed in section 6 below.

Optical (Hipparcos) minus radio (this paper) position differences ($\Delta \alpha \cos \delta, \Delta \delta$) were calculated for the 18 stars on our list (excluding UX Ari) at our 2000.94 epoch. The three rotation angles between the optical and radio frames were determined from these data using a weighted least-squares adjustment (see Table 3). For the radio positions, we used the errors reported in Table 2. For the optical positions we used the Hipparcos errors at epoch (1991.25) updated to our epoch using the Hipparcos proper motion errors. No significant misalignment of the frames was found to within the formal errors of about 3 mas per axis. The reduced χ^2 for the solutions is ≈ 1.0 , confirming the error estimates for the input data.

5. PROPER MOTIONS

The positions of the 19 radio stars from our VLA+PT observations were combined with previous VLA observations (Johnston et al. 1985; Johnston, de Vegt & Gaume 2003) to determine stellar proper motions, $\mu_{\alpha \cos \delta}$ and μ_{δ} , for the 15 sources common to both programs. Although the data cover a long time range, 1978–2000, the sampling is not sufficient to enable the determination of source parallaxes. We therefore computed proper motions for the 15 stars using the parallaxes obtained from Hipparcos. The proper motions derived from the combined VLA and VLA+PT data are listed in Table 4. The values listed in columns 3 and 4 of Table 4 were computed using a linear least-squares fit to the data weighted by the position errors for each observation. Position errors for the previous VLA

observations were estimated to be 30 mas in both $\alpha \cos \delta$ and δ (Johnston, de Vegt & Gaume 2003) and we have adopted these values in our proper motion analysis. We did not attempt to include accelerations or to model possible companions in wide orbits with the exception of the star UX Ari discussed in the next section.

In addition to our VLA/VLA+PT proper motions, Table 4 lists the proper motions derived from the Hipparcos mission and from long-term VLBI observations by Lestrade et al. (1999). Comparing the various proper motions listed in the table, one can see that the VLA/VLA+PT values, with mean errors of 1.44 mas yr^{-1} in $\mu_{\alpha \cos \delta}$ and 1.79 mas yr^{-1} in μ_{δ} , are beginning to approach the accuracies of the Hipparcos proper motions with mean errors of 0.95 mas yr^{-1} and 0.87 mas yr^{-1} respectively. For a few of the stars listed in Table 4, our proper motion errors are actually smaller than those derived from the Hipparcos observations.

Comparisons of the VLA/VLA+PT proper motions with those derived from Hipparcos and VLBI data are shown in Figures 7 and 8. Figure 7 plots the differences between the proper motions in $\alpha \cos \delta$ ($\Delta \mu_{\alpha \cos \delta}$) and δ ($\Delta \mu_{\delta}$), as derived from our VLA/VLA+PT observations and those of Hipparcos. The error bars are the root-sum-square of the uncertainties reported for the two sets of proper motions. For six of the 15 stars common to both data sets, proper motions in both $\alpha \cos \delta$ and δ are in agreement to within the error bars. An additional three stars agree in $\mu_{\alpha \cos \delta}$ only, four stars agree in μ_{δ} only, and two stars do not agree at the 1σ level. Figure 8 shows a similar comparison of the VLA/VLA+PT proper motions with those derived from VLBI observations of Lestrade et al. (1999). Although the errors reported for the VLBI proper motions are significantly smaller than those estimated for the VLA/VLA+PT data (see Table 4), the computed proper motions are in complete agreement for four of the six stars common to both experiments. The other two stars do not agree within the uncertainties in either $\mu_{\alpha \cos \delta}$ or μ_{δ} . One of these stars is Algol a known ternary, for which we only have 6 data points. The other star is UX Ari which was mentioned previously as having large differences between our VLA+PT position and the Hipparcos position. UX Ari is discussed in more detail below.

Finally, in columns 9 and 10 of Table 4 we combined the VLA/VLA+PT, Hipparcos, and VLBI values by computing weighted mean proper motions and associated errors for each of the 15 stars having VLA/VLA+PT data. The combined position was weighted by the errors in the individual proper motions derived from each of the three data sets: VLA/VLA+PT, Hipparcos, and VLBI (when available). The error in the combined position is just the WRMS of the available VLA/VLA+PT, Hipparcos, and/or VLBI errors. Because of the relatively small errors in the VLBI derived proper motions, some of the combined proper motions are heavily weighted toward the VLBI value (see σ^2 CrB for example). The accuracies of the averaged proper motions exceed those of the VLA/VLA+PT and Hipparcos data alone with average WRMS errors of 0.47 mas yr^{-1} in $\mu_{\alpha \cos \delta}$ and 0.48 mas yr^{-1} in μ_{δ} .

6. MOTION OF UX ARIETIS

UX Ari is an active RS CVn binary with an orbital period of 6.44 days and an inclination of $\approx 60^\circ$. Despite being the most observed source in our study, the star UX Ari exhibited unexpectedly large position offsets between our VLA+PT measurements and those derived from the Hipparcos mission. We

scrutinized the reduction and analysis of the VLA+PT data for UX Ari, and could find no errors in the processing. The positions determined for UX Ari when phase-referenced independently to the primary and secondary ICRF calibrators agreed to within 10 mas in $\alpha \cos \delta$ and 1 mas in δ . In addition, the VLA+PT position of the secondary calibrator phase-referenced to the primary calibrator agreed with the "true" ICRF position to within 8 mas in $\alpha \cos \delta$ and 1 mas in δ .

Figure 9 plots the 14 astrometric position measurements derived from our VLA/VLA+PT observations in $\alpha \cos \delta$ and δ from 1978–2000. Because a linear least-squares fit provided a poor representation of the data, we decided to include acceleration terms in the least-squares fits to the time series for UX Ari. These fits are shown as solid curves in Figure 9. Central epochs of 1985.2922 in right ascension and 1985.2311 in declination were computed, and the data were fit with a second order polynomial using a weighted least-squares method. The linear terms in the fits represent the proper motions which are reported in the additional row for UX Ari in Table 4. The second order terms represent the accelerations obtained from the fit, which are $-0.60 \pm 0.03 \text{ mas yr}^{-2}$ in $\alpha \cos \delta$ and $-0.31 \pm 0.02 \text{ mas yr}^{-2}$ in δ .

It should not be too surprising that the observed motion for UX Ari consists of more than just linear proper motion. Lestrade et al. (1999) reported statistically significant accelerations of $-0.54 \pm 0.07 \text{ mas yr}^{-2}$ (8σ) in $\alpha \cos \delta$ and $-0.29 \pm 0.07 \text{ mas yr}^{-2}$ (4σ) in δ for their VLBI observations. These accelerations are in very good agreement with the accelerations derived from our VLA/VLA+PT data. Lestrade et al. (1999) suggested that these accelerations might be due to the gravitational influence of a companion and, if bound, the wider components should have an orbital period many times the 11-year span of their data. The RS CVn system does, in fact, have a companion, and UX Ari is listed in the Washington Double Star catalog (Mason et al. 2001) with the designation WDS 03266+2843. The separation between the RS CVn system and the third star has been measured several times using speckle interferometry, most recently by Hartkopf et al. (2000) who measured a separation of $0''.256$ at an epoch of 1996.8658. In addition, spectroscopic radial velocity measurements of the RS CVn components by Duemmler & Aarum (2001) show a systematic variation of the center of mass velocity with time indicating the influence of a third star. Their preliminary fits to the radial velocity measurements yielded periods of approximately 10.7 and 21.5 years for circular and elliptical orbits respectively.

A fit to the very limited data in the WDS (W. I. Hartkopf 2002, private communication) yielded an orbital period of $51.1 \pm 24.8 \text{ yr}$, a semimajor axis of $0''.34 \pm 0''.11$, and an inclination of $94.4^\circ \pm 3.5^\circ$ for the third component of the system. This period is significantly longer than those determined from the radial velocity measurements and more in line with expectations given the accelerations derived for the RS CVn system from the VLBI measurements of Lestrade et al. (1999) and the VLA/VLA+PT data here. The inclination angle estimated from the WDS data is significantly tilted with respect to inclination angle of the RS CVn orbit of $\approx 60^\circ$. Assuming the period and semimajor axis from the WDS orbit, the total mass of the system is determined to be $\approx 1.9M_\odot$, which is slightly less than the mass of the RS CVn system alone ($m_{1,2} = 2.05M_\odot$) given in Duemmler & Aarum (2001). A second fit to the WDS data assuming an inclination for the outer orbit equal to that of the RS CVn system (C. A. Hummel 2002, private communication)

yielded a smaller semimajor axis, a shorter period, and an eccentricity close to 1. The total mass for this orbit is again less than the assumed mass of the RS CVn component of the system. The total system masses determined from the fits to the WDS data clearly do not agree with the mass of the RS CVn system, and probably reflect limitations in the orbits determined from the sparse data. Additional observations would be very helpful in determining a better orbit for the third component of UX Ari and the total mass of the system.

7. DISCUSSION

We have determined the astrometric positions for 19 radio stars using the VLA+PT configuration. The positions presented here, with uncertainties on the order of 10 mas or better, represent a factor of three improvement over the previous VLA results (Johnston et al. 1985; Johnston, de Vegt & Gaume 2003). Stellar positions from Hipparcos are degrading with time due to errors in the Hipparcos proper motions on the order of 1 mas yr^{-1} and due to unmodeled rotations in the frame with respect to the extragalactic objects estimated to be 0.25 mas yr^{-1} per axis. Taking into account these uncertainties, for many of the stars in our list, our VLA+PT positions are better than the corresponding Hipparcos positions at epoch. The proper motions derived from our VLA+PT observations combined with previous VLA data of Johnston, de Vegt & Gaume have errors which are on the order of, and in some cases are better than, those obtained from Hipparcos.

To our knowledge we provide here the first critical check on the Hipparcos frame to ICRF alignment after the initial effort in the mid 1990's. The formal, predicted error on the frame alignment at our epoch of 2000.94, thus 9.69 years after the mean Hipparcos epoch of 1991.25, is 2.5 mas. Our observations indicate insignificant alignment rotations of $\leq 2.3 \text{ mas}$ with a formal error of $\approx 3 \text{ mas}$ per axis. In a pilot investigation, 172 extragalactic sources were used to compare the ICRF/optical frames (Assafin et al. 2003, AJ, in press). This program yielded similar results with no significant system rotations found and formal errors on the 3 mas level. However, systematic errors in the preliminary, wide-field, optical data of $\approx 10 \text{ mas}$ were reported. For determining possible radio/optical frame differences the use of radio stars is currently more competitive because the accurate Hipparcos data can be utilized directly.

Although future astrometric satellite missions will likely observe distant extragalactic objects directly to provide a tie to the radio reference frame, astrometric observations of radio stars will still provide an important verification of such a link as demonstrated here. It is possible that on the proposed microarcsecond scales measurable by future astrometric satellites, the extragalactic sources may have significant time dependent source structure affecting quasar optical positions. This is indeed the case on milliarcsecond levels at radio wavelengths as shown by Fey & Charlot (1997) and Fey & Charlot (2000).

The VLA+PT configuration provides a useful tool for radio-star astrometry because of its ability to do both high resolution and high sensitivity observations at the same time. Compared with the 24 hour VLA+PT observing time, the same 19 stars plus phase calibrator sources would have taken on the order of 120 hours of time on the VLBA. To observe the 50 stars in the Johnston, de Vegt & Gaume list at multiple epochs using the VLBA would require a tremendous allocation of time, and such a project is probably impractical. Clearly additional observations are necessary to update the positions and proper motions

of the 50 radio stars previously observed with the VLA especially since the VLA+PT configuration offers a factor of three improvement over the previous measurements. Additional observations, with better sampling in time, will also enable the determination of the parallaxes directly from the radio data.

There are several areas in which we might extend or improve our radio-star astrometry in future experiments. As mentioned in section 3, our use of the dirty rather than CLEANed images to determine the positions may have been unnecessarily conservative, since there was little difference between the positions derived from the two sets of images. In Figure 2 there was a slight increase in position error as a function of decreasing source elevation likely due to unmodeled atmospheric and ionospheric effects. Modeling of the phase fluctuations due to these phenomena may result in improved astrometric positions. Observationally, the use of fast-switching and two phase calibrators per target star proved to be beneficial in our analysis of the data and worth the additional observation time. In future experiments, it may be useful to increase the number of observa-

tions per star to a number greater than the three we used for this experiment. For example, Johnston, de Vegt & Gaume (2003) used 5–6 observations per star in their VLA radio-star astrometry. The three observations per star used here was the result of a compromise between our desire for better uv coverage and the scheduling constraints imposed by the use of fast-switching and the VLA+PT configuration. Finally, the greatest improvements in stellar astrometry at radio wavelengths will likely come from future enhancements to the VLA. The increased sensitivity of Phase I of the EVLA project will extend the total number of stars observable with the VLA and will shorten time required to observe these stars. Phase II of the EVLA project will further increase the resolution provided by the VLA+PT configuration with the addition of up to 8 new antennas at distances of up to 300 km from the VLA.

The authors would like to thank Dr. William Hartkopf and Dr. Christian Hummel for providing orbital fits to the WDS data for the star UX Ari.

REFERENCES

- Carilli, C. L., & Holdaway, M. A. 1997, VLA Scientific Memo, 173, 1
 Claussen, M. J, Beresford, R., Sowinski, K. & Ulvestad, J. S. 1999, BAAS, 195, 83.05
 Duemmler, R., & Aarum, V. 2001, A&A, 370, 974
 Fey, A. L., & Charlot, P. 1997, ApJS, 111, 95
 Fey, A. L., & Charlot, P. 2000, ApJS, 128, 17
 Hartkopf, W. I., et al. 2000, AJ, 119, 3084
 IERS Annual Report 1999, ed. D. Gambis, Observatoire de Paris, VI, 87
 Johnston, K. J., Wade, C. M., Florkowski, D. R., & de Vegt, C. 1985, AJ, 90, 1343
 Johnston, K. J., de Vegt, C., & Gaume, R. A. 2003, AJ, in press.
 Kovalevsky, J., et al. 1997, A&A, 323, 620
 Lestrade, J.-F, Preston, R. A., Jones, D.L., Phillips, R. B., Rogers, A. E. E., Titus, M. A., Rioja, M. J., & Gabuzda, D. C. 1999, A&A, 344, 1014
 Ma, C., et al. 1998, AJ, 116, 516
 Mason, B. D., Wycoff, G. L., Hartkopf, W. I., Douglass, G. G., & Worley, C. E. 2001, AJ, 122, 3466
 Perryman M. A. C., et al. 1997, A&A, 323, L49

Figure Captions

FIG. 1.— Distribution of the 19 observed radio stars plotted on an Aitoff equal-area projection of the celestial sphere. The dotted line represents the Galactic equator.

FIG. 2.— Formal errors from the 2-D Gaussian fits to the dirty images for each observation plotted as a function of source elevation. Errors in $\alpha \cos \delta$ are plotted in (a) and errors in declination are plotted in (b).

FIG. 3.— Differences between the ICRF reference positions and our VLA+PT measured positions as a function of source right ascension α for the 38 observed quasars. Differences in $\alpha \cos \delta$ are plotted in (a) and differences in declination δ are plotted in (b). Error bars are from our VLA+PT measurements.

FIG. 4.— Differences between the ICRF reference positions and our VLA+PT measured positions as a function of source declination δ for the 38 observed quasars. Differences in $\alpha \cos \delta$ are plotted in (a) and differences in declination are plotted in (b). Error bars are from our VLA+PT measurements.

FIG. 5.— Differences between the Hipparcos positions updated to the epoch of our observations, and our VLA+PT measured positions as a function of source right ascension α for the 19 radio stars observed. Differences in $\alpha \cos \delta$ are plotted in (a) and differences in declination are plotted in (b). Error bars are from our VLA+PT measurements.

FIG. 6.— Differences between the Hipparcos positions updated to the epoch of our observations, and our VLA+PT measured positions as a function of source declination δ for the 19 radio stars observed. Differences in $\alpha \cos \delta$ are plotted in (a) and differences in declination are plotted in (b). Error bars are from our VLA+PT measurements.

FIG. 7.— Differences in the proper motions, $\Delta\mu_{\alpha \cos \delta}$ vs. $\Delta\mu_{\delta}$, as derived from our VLA+PT observations and from the Hipparcos mission. Error bars are the root-sum-square of the errors give in Table 4 for the two measurement sets.

FIG. 8.— Differences in the proper motions, $\Delta\mu_{\alpha \cos \delta}$ vs. $\Delta\mu_{\delta}$, as derived from our VLA+PT observations and the VLBI observations of Lestrade et al. (1999). Error bars are the root-sum-square of the errors give in Table 4 for the two measurement sets.

FIG. 9.— Proper motions for the star UX Ari in (a) right ascension and (b) declination estimated from our VLA+PT observations and the VLA data of Johnston, de Vegt & Gaume (2003). The solid curve represents a weighted least-squares fit of a second order polynomial to the data. Errors for the Johnston, de Vegt & Gaume VLA data are 30 mas in both $\alpha \cos \delta$ and δ .

TABLE 1
RADIO STARS AND THEIR CORRESPONDING ICRF REFERENCE SOURCES.

Star	Hipparcos Number	Reference Source ^a	ICRF Designation ^b	α (J2000) ^c (h m s)	δ (J2000) ^c ($^{\circ}$ ' ")	Separation ($^{\circ}$)
LSI61303	12469	0302+625	C	03 06 42.659558	62 43 02.02417	3.5
		0241+622	C	02 44 57.696827	62 28 06.51459	1.3
Algol	14576	0309+411	D	03 13 01.962129	41 20 01.18353	1.0
		0248+430	D	02 51 34.536779	43 15 15.82858	3.9
UX Ari	16042	0333+321	O	03 36 30.107599	32 18 29.34239	4.2
		0326+277	O	03 29 57.669413	27 56 15.49914	1.1
HR1099	16846	0336-019	C	03 39 30.937787	-01 46 35.80399	2.5
		0305+039	N	03 08 26.223804	04 06 39.30105	7.9
B Per	20070	0420+417	C	04 23 56.009795	41 50 02.71277	8.5
		0300+470	O	03 03 35.242226	47 16 16.27546	12.3
T Tau	20390	0409+229	N	04 12 43.666851	23 05 05.45299	4.2
		0400+258	D	04 03 05.586048	26 00 01.50274	7.9
α Ori	27989	0611+131	C	06 13 57.692766	13 06 45.40116	7.4
		0529+075	C	05 32 38.998531	07 32 43.34586	5.6
HD50896-N	33165	0646-306	C	06 48 14.096441	-30 44 19.65940	6.9
		0727-115	O	07 30 19.112472	-11 41 12.60048	14.8
KQ Pup	36773	0727-115	O	07 30 19.112472	-11 41 12.60048	3.0
		0733-174	D	07 35 45.812508	-17 35 48.50131	3.1
54 Cam	39348	0749+540	D	07 53 01.384573	53 52 59.63716	3.6
		0831+557	D	08 34 54.903997	55 34 21.07080	4.7
TY Pix-N	44164	0925-203	C	09 27 51.824323	-20 34 51.23266	9.5
		0919-260	O	09 21 29.353874	-26 18 43.38604	5.0
RS CVn	64293	1308+326	D	13 10 28.663845	32 20 43.78295	3.6
		1404+286	O	14 07 00.394410	28 27 14.68998	13.6
HR5110	66257	1315+346	C	13 17 36.494189	34 25 15.93266	4.4
		1404+286	O	14 07 00.394410	28 27 14.68998	10.8
δ Lib	73473	1511-100	C	15 13 44.893444	-10 12 00.26435	3.6
		1510-089	O	15 12 50.532939	-09 05 59.82950	3.0
σ^2 CrB	79607	1611+343	C	16 13 41.064249	34 12 47.90909	0.4
		1600+335	D	16 02 07.263468	33 26 53.07267	2.6
β Lyra	92420	1901+319	O	19 02 55.938870	31 59 41.70209	3.0
		1751+288	O	17 53 42.473634	28 48 04.93908	12.6
HD199178	103144	2037+511	D	20 38 37.034755	51 19 12.66269	7.5
		2100+468	C	21 02 17.056042	47 02 16.25451	3.0
AR Lac	109303	2200+420	O	22 02 43.291377	42 16 39.97994	3.6
		2214+350	C	22 16 20.009910	35 18 14.18056	10.5
IM Peg	112997	2250+190	N	22 53 07.369176	19 42 34.62843	2.9
		2251+158	O	22 53 57.747932	16 08 53.56089	0.7

^aFor each star the primary (fast-switched) reference source is listed first followed by the secondary reference source.

^bICRF source designation (IERS Annual Report 1999): D = defining, C = candidate, O = other, N = new in ICRF Extension 1.

^cICRF Extension 1 source positions (IERS Annual Report 1999).

TABLE 2
SOURCE POSITIONS ESTIMATED FROM THE VLA+PT DATA

Source ^a	α (J2000) (h m s)	δ (J2000) ($^{\circ}$ ' ")	S (mJy)	S.N.R.
LSI61303	02 40 31.6646 \pm 0.0008 (\pm 0.006")	61 13 45.593 \pm 0.003	42.2	227.8
0302+625	03 06 42.6598 \pm 0.0004 (\pm 0.003")	62 43 02.026 \pm 0.004	242.6	123.8
0241+621	02 44 57.6972 \pm 0.0021 (\pm 0.014")	62 28 06.512 \pm 0.008	605.9	142.6
Algol	03 08 10.1307 \pm 0.0001 (\pm 0.001")	40 57 20.345 \pm 0.007	24.2	101.5
0309+411	03 13 01.9622 \pm 0.0013 (\pm 0.014")	41 20 01.186 \pm 0.004	454.5	132.5
0248+430	02 51 34.5361 \pm 0.0010 (\pm 0.011")	43 15 15.824 \pm 0.006	893.8	113.6
UX Ari	03 26 35.3849 \pm 0.0006 (\pm 0.008")	28 42 54.176 \pm 0.004	10.1	121.7
0333+321	03 36 30.1063 \pm 0.0006 (\pm 0.008")	32 18 29.347 \pm 0.005	1515.4	153.6
0326+277	03 29 57.6700 \pm 0.0008 (\pm 0.011")	27 56 15.500 \pm 0.005	613.1	121.4
HR1099	03 36 47.2869 \pm 0.0003 (\pm 0.005")	00 35 15.772 \pm 0.005	13.5	204.1
0336-019	03 39 30.9380 \pm 0.0014 (\pm 0.020")	-01 46 35.785 \pm 0.034	1798.1	99.8
0305+039	03 08 26.2240 \pm 0.0011 (\pm 0.016")	04 06 39.288 \pm 0.026	562.6	84.7
B Per	04 18 14.6216 \pm 0.0014 (\pm 0.014")	50 17 43.766 \pm 0.021	0.4	10.5
0420+417	04 23 56.0106 \pm 0.0008 (\pm 0.009")	41 50 02.720 \pm 0.007	1040.2	61.0
0300+470	03 03 35.2409 \pm 0.0015 (\pm 0.015")	47 16 16.259 \pm 0.008	987.6	69.6
T Tau-N	04 21 59.4345 \pm 0.0004 (\pm 0.005")	19 32 06.406 \pm 0.009	1.1	21.6
T Tau-S	04 21 59.4258 \pm 0.0005 (\pm 0.007")	19 32 05.718 \pm 0.008	6.1	131.4
0409+229	04 12 43.6669 \pm 0.0005 (\pm 0.007")	23 05 05.445 \pm 0.009	326.5	114.4
0400+258	04 03 05.5854 \pm 0.0008 (\pm 0.010")	26 00 01.503 \pm 0.003	884.0	69.6
α Ori	05 55 10.3061 \pm 0.0009 (\pm 0.013")	07 24 25.432 \pm 0.026	2.8	50.2
0611+131	06 13 57.6933 \pm 0.0020 (\pm 0.029")	13 06 45.401 \pm 0.006	266.2	48.6
0529+075	05 32 39.0000 \pm 0.0017 (\pm 0.025")	07 32 43.336 \pm 0.024	903.4	56.2
HD50896-N	06 54 13.0456 \pm 0.0031 (\pm 0.043")	-23 55 41.993 \pm 0.107	1.1	22.3
0646-306	06 48 14.1014 \pm 0.0017 (\pm 0.022")	-30 44 19.634 \pm 0.027	527.7	28.5
0727-115	07 30 19.1085 \pm 0.0018 (\pm 0.026")	-11 41 12.589 \pm 0.100	2026.6	24.0
KQ Pup	07 33 47.9637 \pm 0.0002 (\pm 0.002")	-14 31 25.994 \pm 0.007	2.3	41.7
0727-115	07 30 19.1124 \pm 0.0016 (\pm 0.023")	-11 41 12.607 \pm 0.008	3869.7	44.8
0733-174	07 35 45.8133 \pm 0.0006 (\pm 0.008")	-17 35 48.483 \pm 0.010	1002.5	49.7
54 Cam	08 02 35.7815 \pm 0.0012 (\pm 0.010")	57 16 24.997 \pm 0.005	1.1	26.4
0749+540	07 53 01.3851 \pm 0.0014 (\pm 0.012")	53 52 59.632 \pm 0.029	854.6	105.0
0831+557	08 34 54.9023 \pm 0.0014 (\pm 0.012")	55 34 21.079 \pm 0.014	2641.6	137.9
TY Pix-N	08 59 42.7205 \pm 0.0003 (\pm 0.005")	-27 48 58.711 \pm 0.014	2.1	40.8
0925-203	09 27 51.8231 \pm 0.0011 (\pm 0.015")	-20 34 51.246 \pm 0.033	325.5	78.4
0919-260	09 21 29.3552 \pm 0.0007 (\pm 0.010")	-26 18 43.370 \pm 0.024	1590.4	72.4
RS CVn	13 10 36.9034 \pm 0.0014 (\pm 0.017")	35 56 05.604 \pm 0.004	1.2	32.3
1308+326	13 10 28.6638 \pm 0.0007 (\pm 0.009")	32 20 43.803 \pm 0.032	1397.0	89.0
1404+286	14 07 00.3940 \pm 0.0017 (\pm 0.022")	28 27 14.679 \pm 0.030	1815.0	99.7
HR5110	13 34 47.8155 \pm 0.0003 (\pm 0.004")	37 10 56.672 \pm 0.010	7.2	116.7
1315+346	13 17 36.4934 \pm 0.0020 (\pm 0.025")	34 25 15.946 \pm 0.039	239.0	82.4
1404+286	14 07 00.3942 \pm 0.0034 (\pm 0.045")	28 27 14.672 \pm 0.040	1715.0	78.0
δ Lib	15 00 58.3456 \pm 0.0009 (\pm 0.013")	-08 31 08.219 \pm 0.018	1.4	37.5
1511-100	15 13 44.8943 \pm 0.0012 (\pm 0.018")	-10 12 00.255 \pm 0.007	813.0	100.4
1510-089	15 12 50.5324 \pm 0.0005 (\pm 0.008")	-09 05 59.837 \pm 0.005	1010.0	120.2
σ^2 CrB	16 14 40.8337 \pm 0.0001 (\pm 0.002")	33 51 30.892 \pm 0.002	12.9	68.0
1611+343	16 13 41.0636 \pm 0.0007 (\pm 0.009")	34 12 47.910 \pm 0.005	4295.0	163.9
1600+335	16 02 07.2638 \pm 0.0006 (\pm 0.007")	33 26 53.073 \pm 0.006	1271.0	198.6
β Lyra	18 50 04.7945 \pm 0.0006 (\pm 0.007")	33 21 45.595 \pm 0.004	4.3	101.7
1901+319	19 02 55.9403 \pm 0.0021 (\pm 0.027")	31 59 41.718 \pm 0.014	1005.0	102.6
1751+288	17 53 42.4723 \pm 0.0016 (\pm 0.022")	28 48 04.925 \pm 0.015	664.0	100.6
HD199178	20 53 53.6544 \pm 0.0006 (\pm 0.007")	44 23 11.080 \pm 0.003	5.0	120.1
2037+511	20 38 37.0331 \pm 0.0017 (\pm 0.016")	51 19 12.655 \pm 0.008	2503.7	160.5

TABLE 2—*Continued*

Source ^a	α (J2000) (h m s)	δ (J2000) ($^{\circ}$ ' '')	S (mJy)	S.N.R.
2100+468	21 02 17.0567 \pm 0.0014 (\pm 0.014'')	47 02 16.265 \pm 0.012	128.8	15.6
AR Lac	22 08 40.8114 \pm 0.0002 (\pm 0.002'')	45 44 32.147 \pm 0.001	3.4	147.1
2200+420	22 02 43.2910 \pm 0.0008 (\pm 0.009'')	42 16 39.974 \pm 0.004	2501.0	188.0
2214+350	22 16 20.0102 \pm 0.0006 (\pm 0.008'')	35 18 14.184 \pm 0.005	465.1	164.9
IM Peg	22 53 02.2638 \pm 0.0003 (\pm 0.004'')	16 50 28.271 \pm 0.016	0.4	120.9
2250+190	22 53 07.3692 \pm 0.0006 (\pm 0.008'')	19 42 34.628 \pm 0.003	414.6	158.9
2251+158	22 53 57.7480 \pm 0.0005 (\pm 0.007'')	16 08 53.559 \pm 0.009	9109.8	198.9

^aFor the three stars HD50896-N, RS CVn, and HR5110, the star's position was determined using the secondary (not fast-switched) ICRF calibrator as the phase reference.

TABLE 3
RADIO/OPTICAL FRAME ALIGNMENT.

Axis	Rotation (mas)	Formal Error (mas)
x ...	-0.2	2.9
y ...	-1.9	3.2
z ...	2.3	2.8

^aMean error of unit weight for the alignment is 9.8 mas, with a reduced χ^2 equal to 0.98.

TABLE 4
COMPARISON OF RADIO-STAR PROPER MOTIONS.

Star	Number of Meas. ^a	VLA/VLA+PT Proper Motions ^b		Hipparcos Proper Motions		VLBI Proper Motions ^c		Combined Proper Motions ^d	
		$\mu_{\alpha \cos \delta}$ (mas yr ⁻¹)	μ_{δ} (mas yr ⁻¹)	$\mu_{\alpha \cos \delta}$ (mas yr ⁻¹)	μ_{δ} (mas yr ⁻¹)	$\mu_{\alpha \cos \delta}$ (mas yr ⁻¹)	μ_{δ} (mas yr ⁻¹)	$\mu_{\alpha \cos \delta}$ (mas yr ⁻¹)	μ_{δ} (mas yr ⁻¹)
LSI61303	1	0.62 ± 1.95	1.63 ± 1.75	0.97 ± 0.26	-1.21 ± 0.32
Algol	6	3.67 ± 0.55	-3.26 ± 0.87	2.39 ± 0.77	-1.44 ± 0.88	2.79 ± 0.14	-0.64 ± 0.18	2.83 ± 0.13	-0.77 ± 0.17
UX Ari	14	38.83 ± 0.54	-105.48 ± 0.54	41.35 ± 1.41	-104.29 ± 1.35	41.23 ± 0.18	-104.01 ± 0.20	40.98 ± 0.17	-104.19 ± 0.19
UX Ari ^e	14	45.64 ± 0.47	-101.84 ± 0.25
HR1099	13	-31.87 ± 0.41	-161.09 ± 0.52	-32.98 ± 0.93	-163.45 ± 0.88	-31.59 ± 0.33	-161.69 ± 0.31	-31.79 ± 0.25	-161.70 ± 0.25
B Per	5	44.24 ± 2.58	-57.33 ± 1.97	46.59 ± 1.17	-56.43 ± 0.94	46.19 ± 1.07	-56.60 ± 0.85
T Tau-N	1	15.45 ± 1.88	-12.48 ± 1.62
α Ori	3	24.17 ± 1.24	10.07 ± 1.81	27.33 ± 2.30	10.86 ± 1.46	24.88 ± 1.09	10.55 ± 1.14
HD50896-N	2	-1.19 ± 1.86	9.32 ± 6.44	-3.86 ± 0.43	4.75 ± 0.66	-3.73 ± 0.42	4.80 ± 0.66
KQ Pup	4	-8.55 ± 1.43	8.24 ± 1.67	-7.73 ± 0.64	3.62 ± 0.53	-7.87 ± 0.58	4.04 ± 0.51
54 Cam	2	-35.34 ± 2.98	-57.13 ± 1.64	-38.28 ± 0.78	-59.08 ± 0.63	-38.10 ± 0.76	-58.83 ± 0.59
TY Pix-N	2	-45.25 ± 1.32	-44.13 ± 1.92	-43.99 ± 0.47	-44.80 ± 0.55	-44.13 ± 0.44	-44.75 ± 0.53
RS CVn	4	-50.61 ± 1.32	27.05 ± 1.52	-49.14 ± 0.88	21.49 ± 0.72	-49.61 ± 0.73	22.51 ± 0.65
HR5110	5	84.53 ± 1.42	-9.38 ± 1.30	84.70 ± 0.45	-9.81 ± 0.39	85.50 ± 0.13	-9.22 ± 0.16	85.43 ± 0.13	-9.31 ± 0.15
δ Lib	4	-66.00 ± 1.84	-5.05 ± 2.35	-66.20 ± 0.86	-3.40 ± 0.81	-66.16 ± 0.78	-3.58 ± 0.77
σ^2 CrB	2	-266.66 ± 1.21	-86.69 ± 1.62	-266.47 ± 0.86	-86.88 ± 1.12	-267.05 ± 0.04	-86.66 ± 0.05	-267.05 ± 0.04	-86.66 ± 0.05
β Lyra	4	2.79 ± 1.38	-5.24 ± 1.18	1.10 ± 0.44	-4.46 ± 0.51	1.26 ± 0.42	-4.58 ± 0.47
HD199178	1	26.77 ± 0.77	-1.15 ± 0.61	26.60 ± 0.41	-1.24 ± 0.43
AR Lac	5	-51.21 ± 1.50	47.96 ± 1.45	-52.48 ± 0.46	47.88 ± 0.53	-52.08 ± 0.13	47.03 ± 0.19	-52.10 ± 0.12	47.14 ± 0.18
IM Peg	1	-20.97 ± 0.61	-27.59 ± 0.57	-20.59 ± 0.46	-27.53 ± 0.40

^aTotal number of position measurements from our VLA+PT observations plus previous VLA observations (Johnston et al. 1985; Johnston, de Vegt & Gaume 2003).

^bProper motions derived from combined VLA and VLA+PT observations.

^cProper motions from Lestrade et al. (1999).

^dWeighted mean of the proper motions from VLA/VLA+PT, Hipparcos, and Lestrade et al. (1999) data.

^eUX Ari proper motions with acceleration terms included.

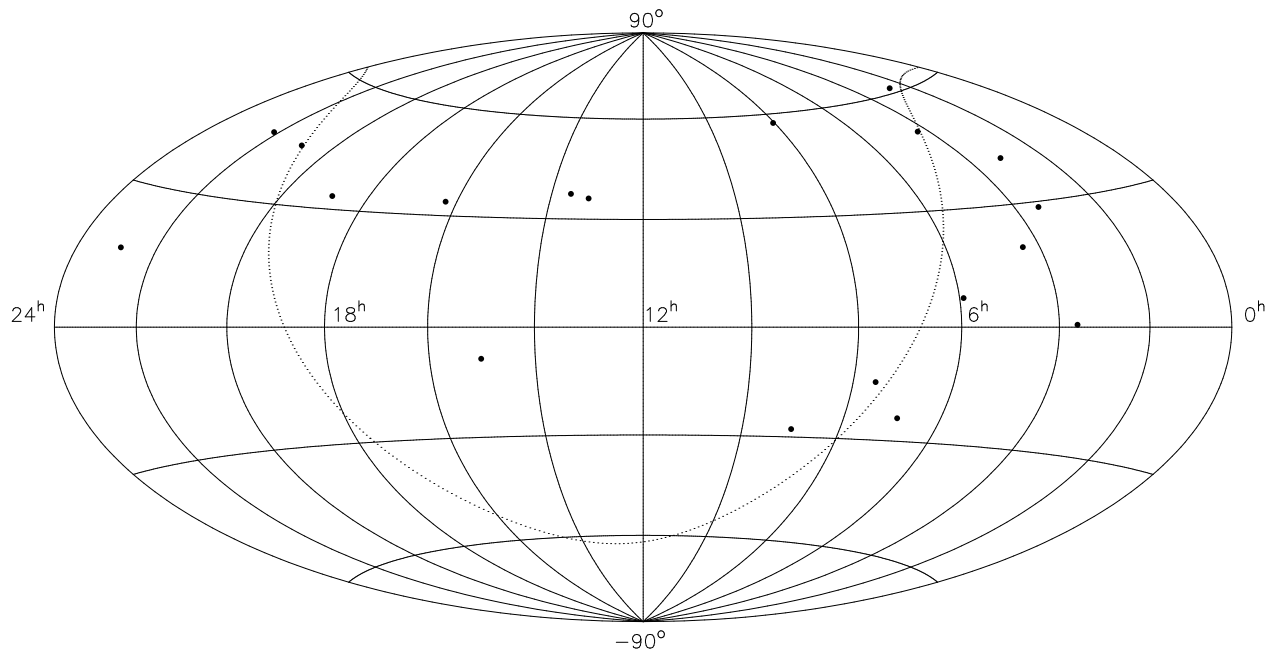


Figure 1

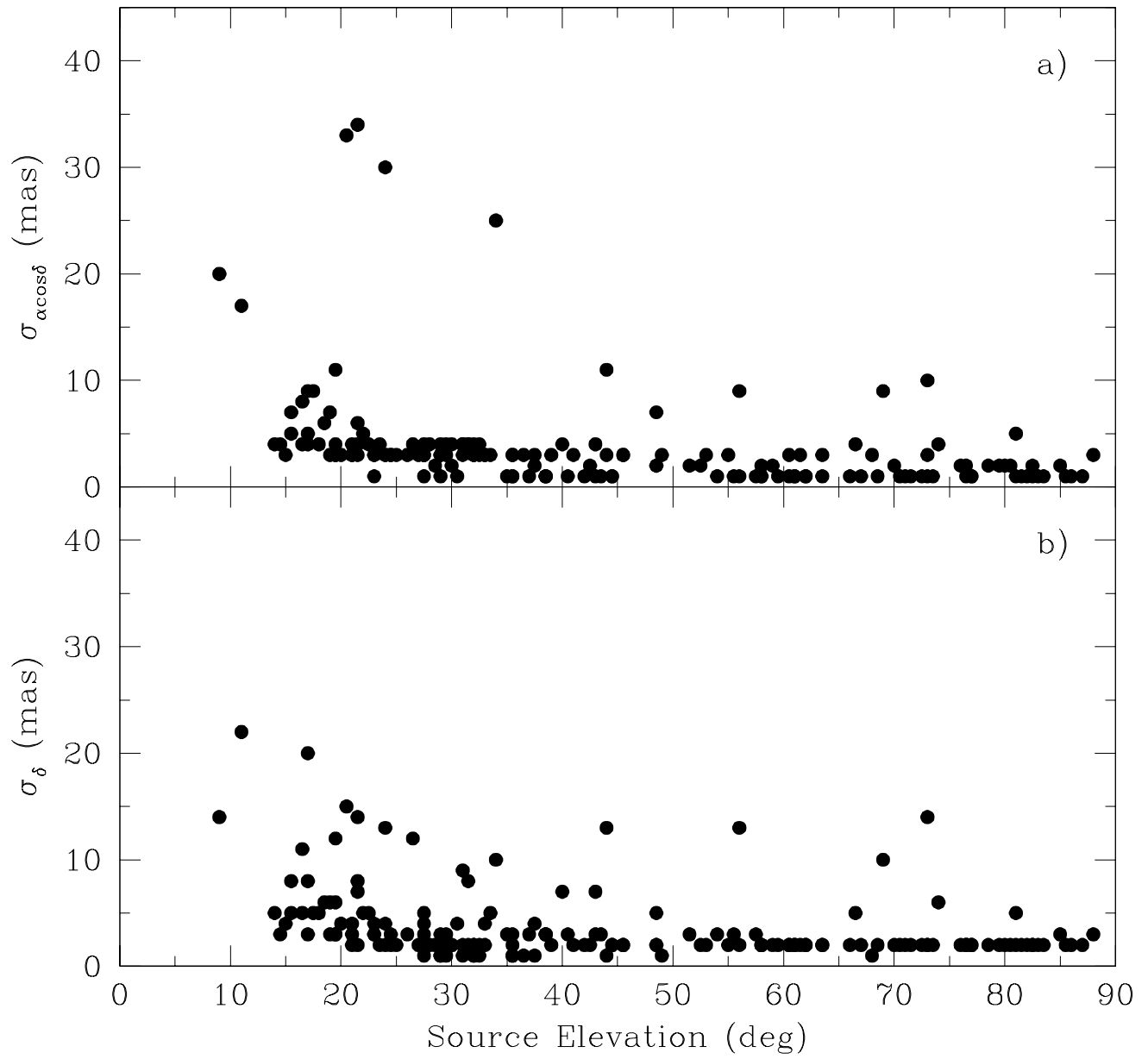


Figure 2

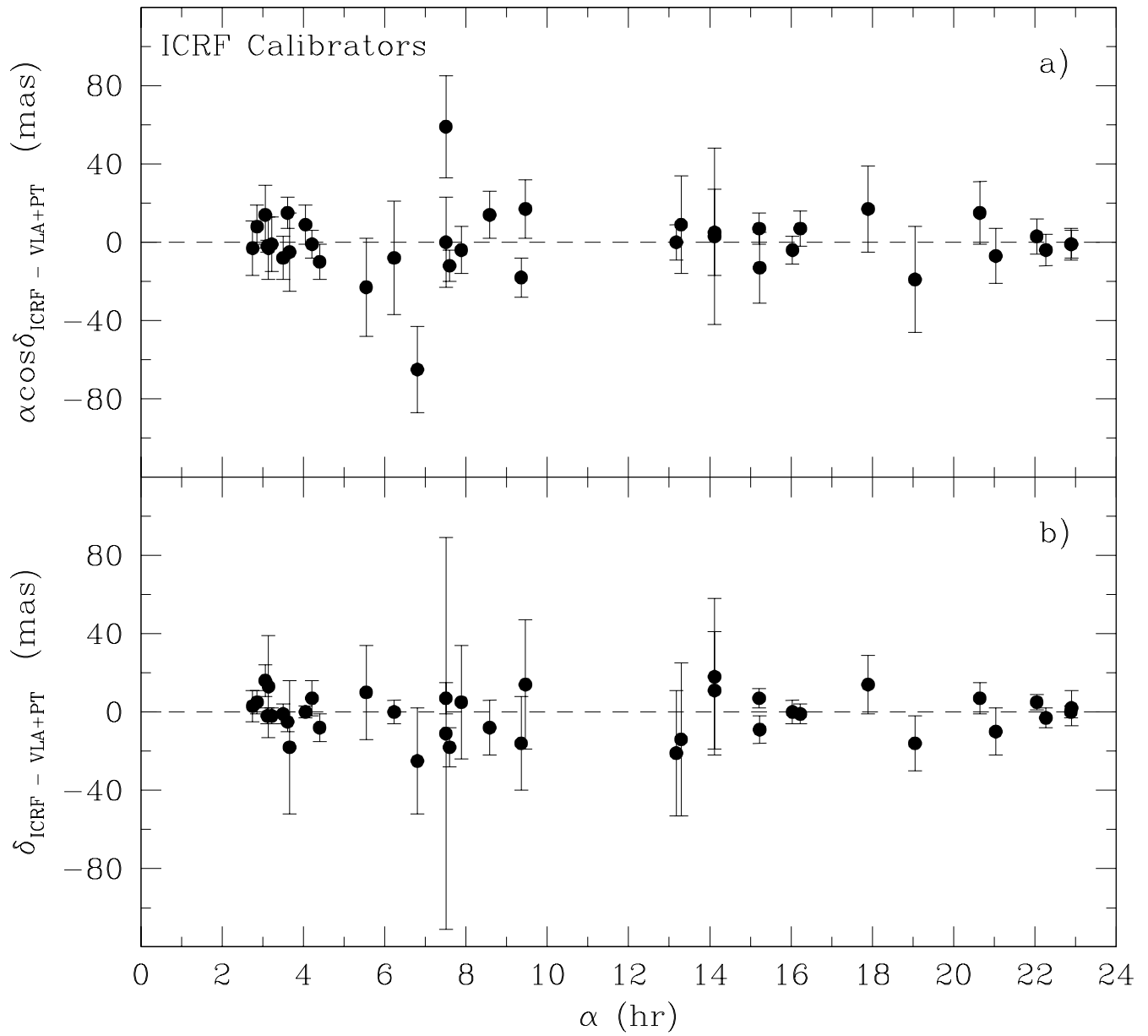


Figure 3

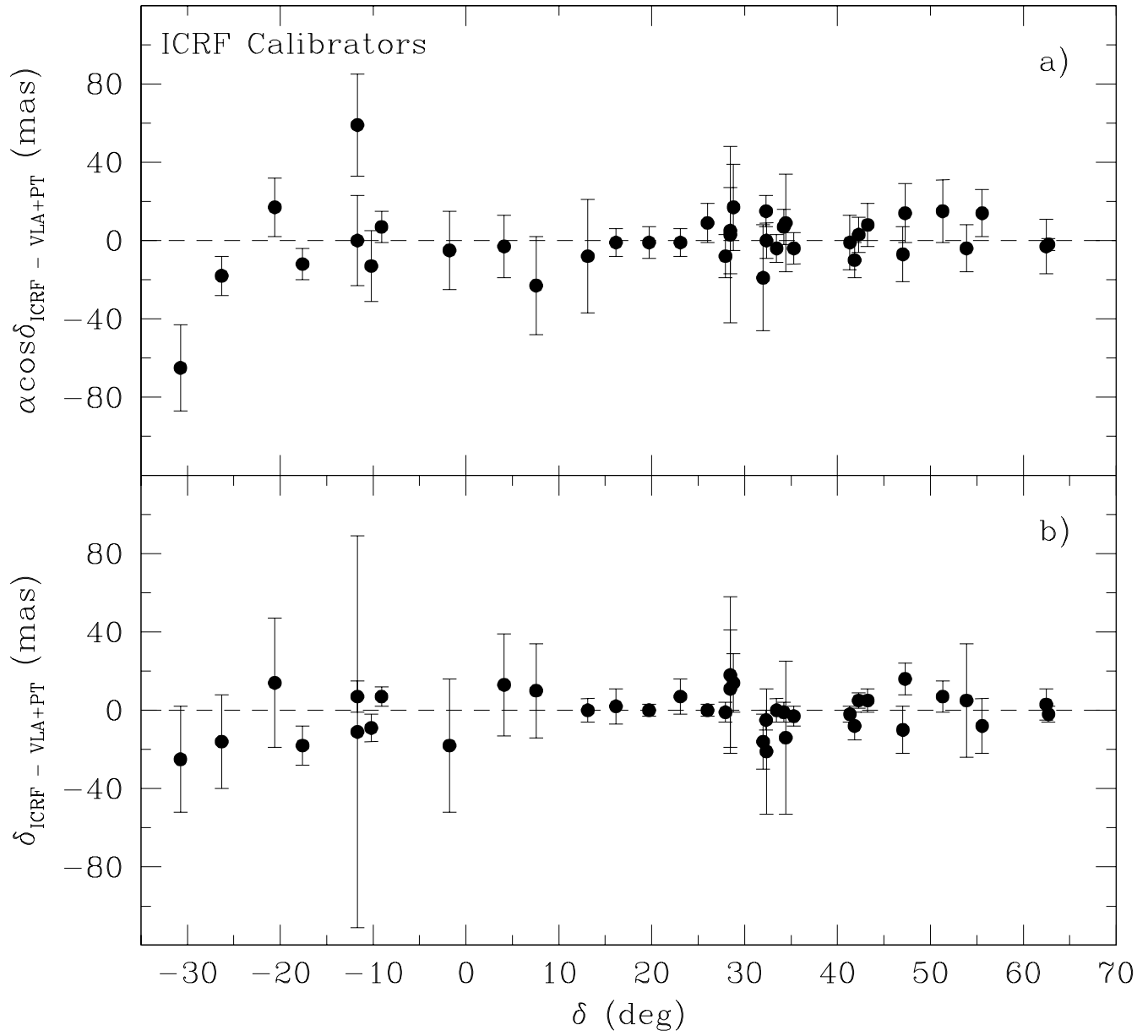


Figure 4

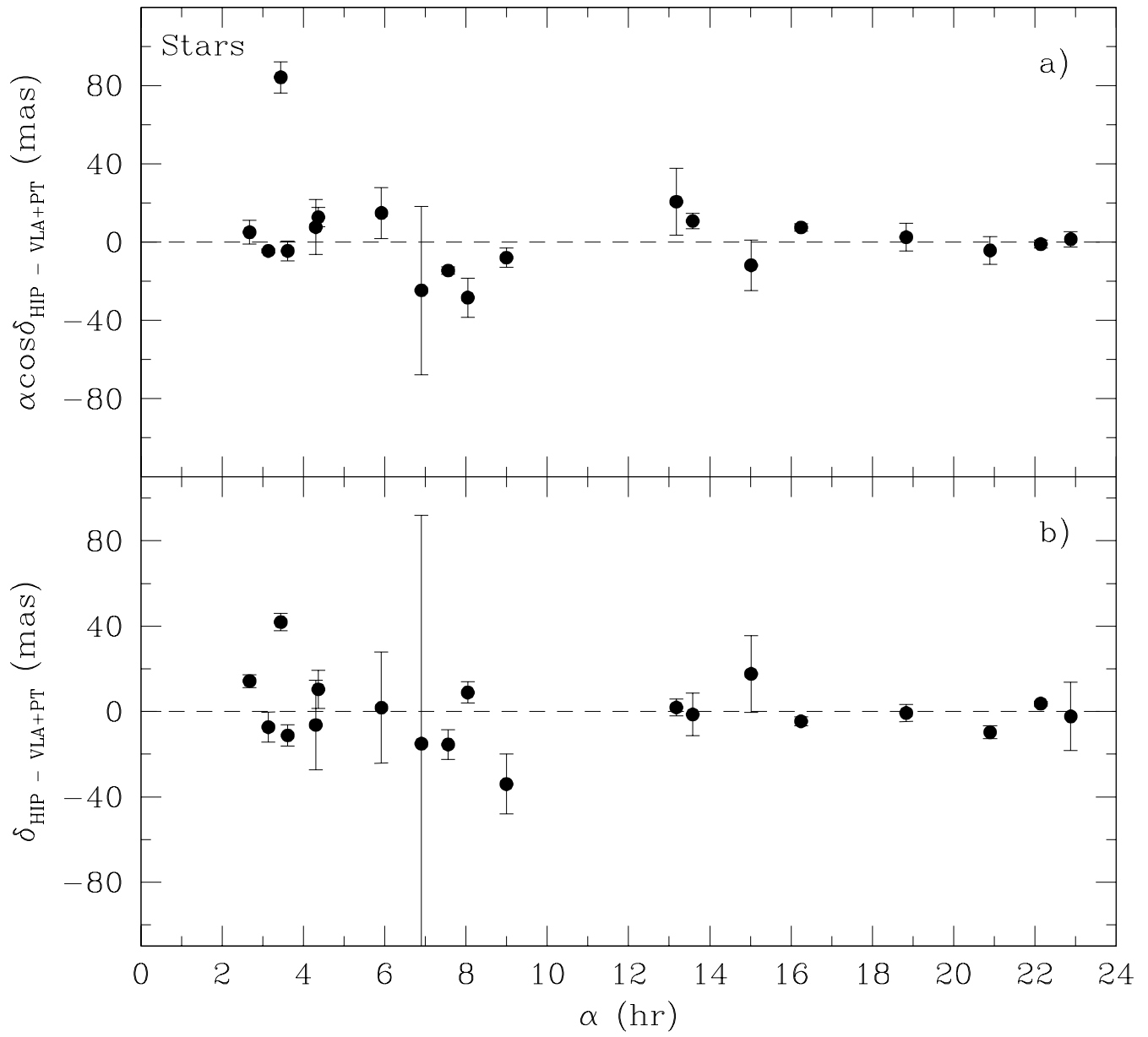


Figure 5

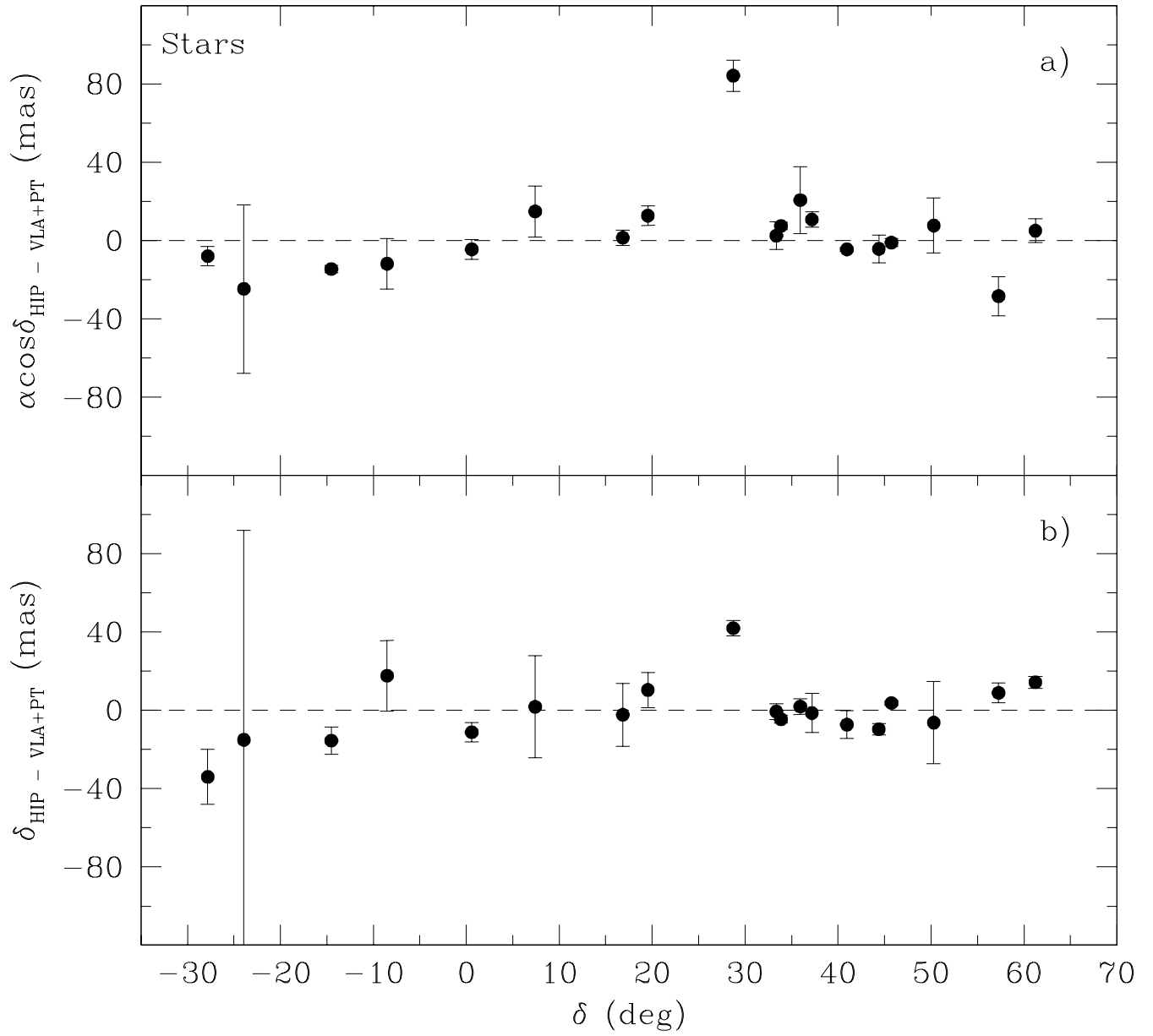


Figure 6

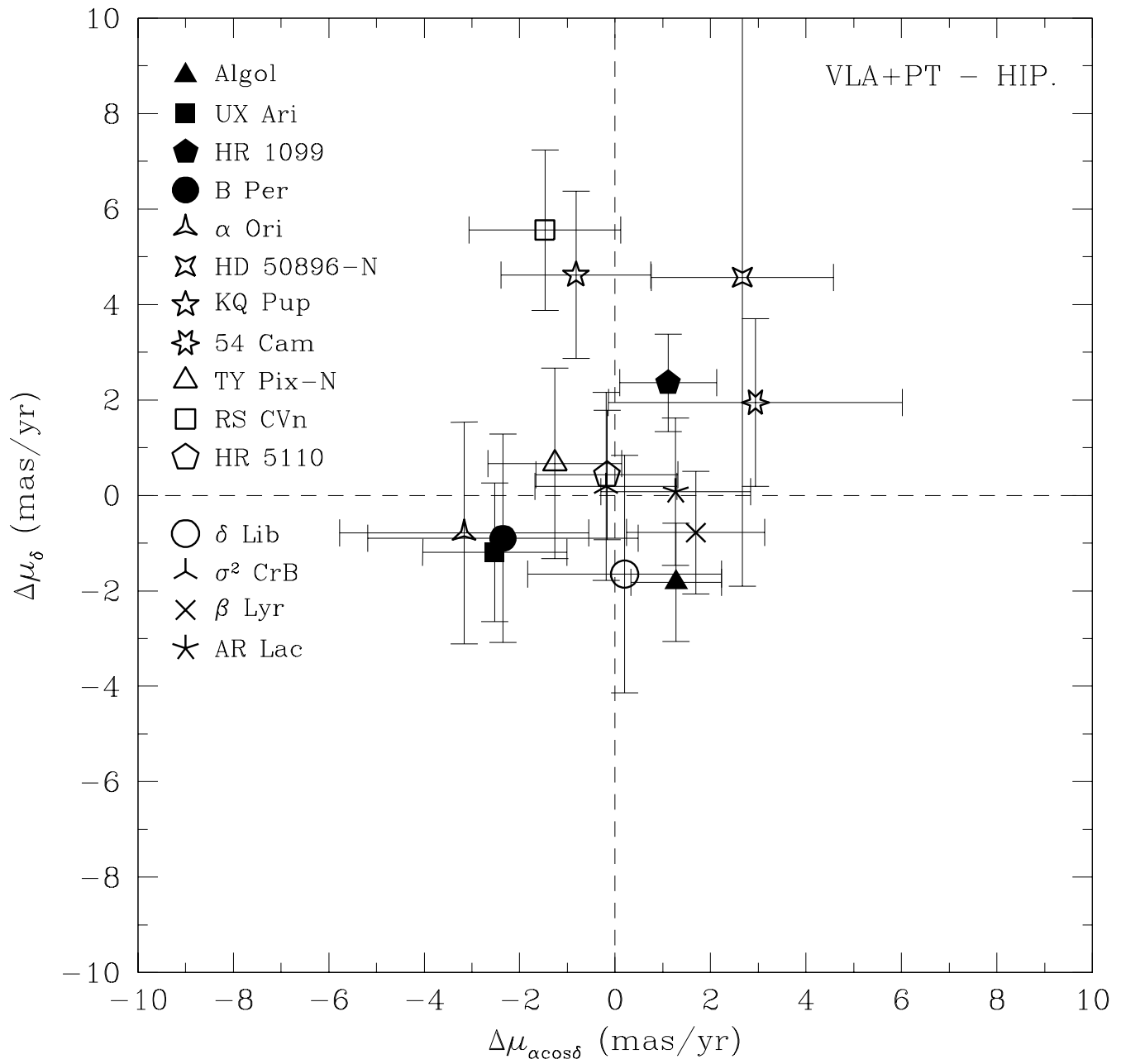


Figure 7

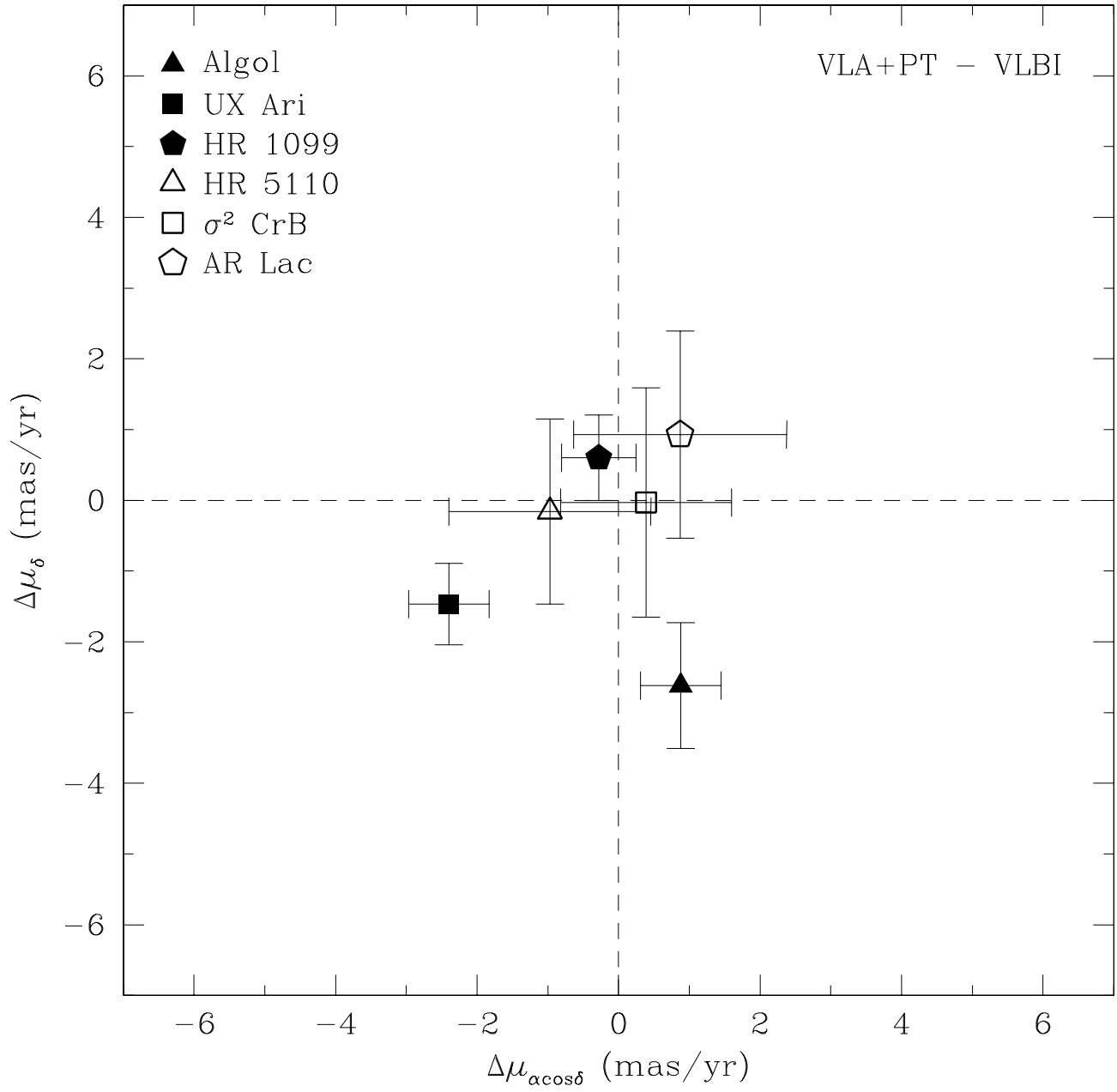


Figure 8

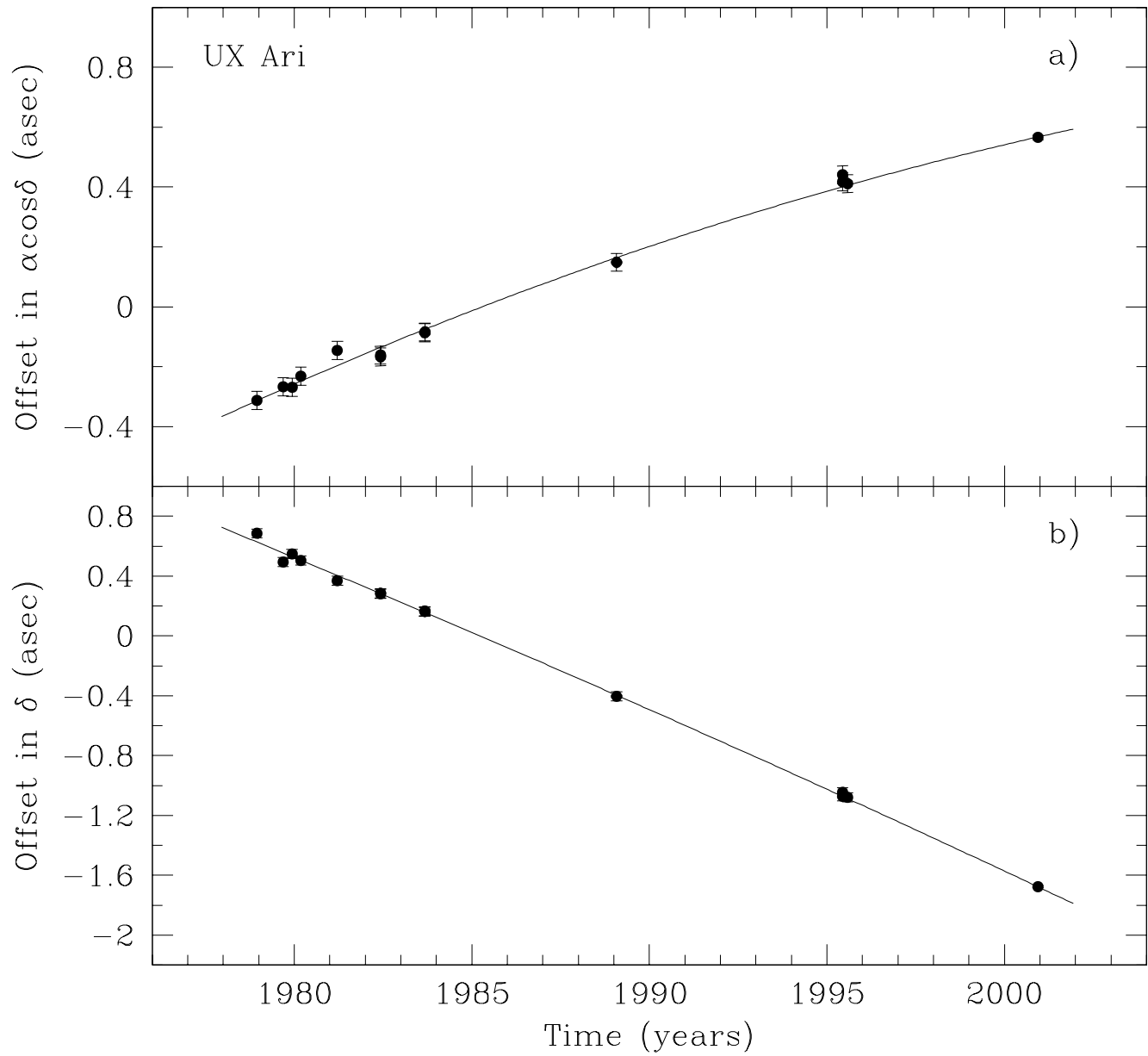


Figure 9